First-principles theory of iron up to earth-core pressures: Structural, vibrational, and elastic properties

Per Söderlind and John A. Moriarty
Department of Physics, Lawrence Livermore National Laboratory, University of California, P.O. Box 808, Livermore, California 94551

John M. Wills
Theoretical Division, Los Alamos National Laboratory, Los Alamos, New Mexico 87545
(Received 2 January 1996)

Ab initio electronic-structure calculations, based on density-functional theory and a full-potential linear-muffin-tin-orbital method, have been used to predict crystal-structure phase stabilities, elastic constants, and Brillouin-zone-boundary phonons for iron under compression. Total energies for five crystal structures, bcc, fcc, bct, hcp, and dhcp, have been calculated over a wide volume range. In agreement with experiment and previous theoretical calculations, a magnetic bcc ground state is obtained at ambient pressure and a nonmagnetic hcp ground state is found at high pressure, with a predicted bcc $\rightarrow$ hcp phase transition at about 10 GPa. Also in agreement with very recent diamond-anvil-cell experiments, a metastable dhcp phase is found at high pressure, which remains magnetic and consequently accessible at high temperature up to about 50 GPa. In addition, the bcc structure becomes mechanically unstable at pressures above 2 Mbar (200 GPa) and a metastable, but still magnetic, bct phase ($c/a \simeq 0.875$) develops. For high-pressure nonmagnetic iron, fcc and hcp elastic constants and fcc phonon frequencies have been calculated to above 4 Mbar. These quantities rise smoothly with pressure, but an increasing tendency towards elastic anisotropy as a function of compression is observed, and this has important implications for the solid inner-core of the earth. The fcc elastic-constant and phonon data have also been used in combination with generalized pseudopotential theory to develop many-body interatomic potentials, from which high-temperature thermodynamic properties and melting can be obtained. In this paper, these potentials have been used to calculate full fcc and hcp phonon spectra and corresponding Debye temperatures as a function of compression. [S0163-1829(96)07221-9]

I. INTRODUCTION

There is growing experimental and theoretical interest in the behavior of the earth's core and the materials physics associated with it. Data from seismology and mineral physics suggest that the core is composed mainly of iron (Fe) or an iron-dominated alloy, but the lack of knowledge of the elastic and vibrational properties of solid iron at inner core pressures (3−4 Mbar) and temperatures (4000−8000 K) have made it hard to interpret the seismological data. Likewise, the high-pressure, high-temperature phase diagram of iron is not well established, with many conflicting experimental results, and not even the stable phase of the solid at inner-core (IC) conditions is known with certainty. Also the high-pressure melting of iron, which leads to the presence of a liquid outer core (OC), is not well understood, with a resulting uncertainty of at least 3000 K in the melting temperature at the IC-OC boundary (see Fig. 1). This has important implications for both the temperature of the inner core and the origin of the geomagnetic field, which is believed to originate from the freezing of the outer Fe core.

As a step towards an improved understanding of the high-pressure physics of Fe, we have performed an extensive series of *ab initio* electronic-structure calculations on the structural, vibrational, and elastic properties of this metal as a function of compression, and we report the results in this paper. These are zero-temperature calculations and range in pressure from ambient to over 4 Mbar. In the high-pressure nonmagnetic limit, we have further used these results to develop many-body interatomic potentials for iron, which can be applied to the study of high-temperature structural and thermodynamic properties, including melting. We also present these potentials here together with some preliminary applications.

Experimentally, there has been considerable recent work on the high-temperature phase diagram and melting curve of

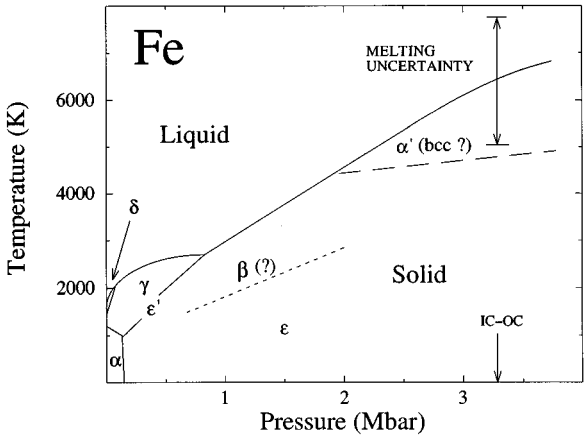

FIG. 1. Possible high-pressure phase diagram of Fe, including established phases α (bcc), γ (fcc), δ (bcc), and ϵ (hcp) as well as proposed new phases ϵ' (dhcp), β (unknown), and α' (proposed bcc).

iron,[1] including indications of undetermined solid phases occurring above 50 GPa (Ref. 2) and above 2 Mbar (200 GPa),[3] respectively, as shown in Fig. 1. The former has been referred to as the β phase, while the latter has been referred to as the α' phase and speculated to be a bcc structure.[4] In very recent laser-heated diamond-anvil-cell experiments, both Saxena *et al.*[5] and Yoo *et al.*[6] report yet another high-temperature structure of iron near 40 GPa and 1500 K, which they identify as dhcp. Saxena *et al.*[5] imply that this dhcp structure is in fact the β phase, but Yoo *et al.*,[6] who previously presented evidence[7] against the existence of the β phase, refer to dhcp as an ϵ' phase existing only *below* 50 GPa. Motivated by these observations, we have studied the phase stability of the bcc, fcc, bct, hcp, and dhcp crystal structures of iron in detail as a function of pressure. In qualitative agreement with other recent calculations,[8,9] we show that the bcc structure is mechanically unstable above 2 Mbar and thus not likely to exist as a high-pressure, high-temperature phase. At the same time, we find that the magnetic bct structure into which bcc evolves at high pressure is a possible candidate for the α' phase. We further show that below 50 GPa the observed dhcp structure is metastable and accessible at high temperature due to its ferromagnetism, but that its magnetic moment drops rapidly to zero at higher pressure. Thus, in agreement with Yoo *et al.*,[6,7] we believe that dhcp is much more likely to be the proposed ϵ' phase than the proposed β phase.

In addition to our study of crystal-structure phase stabilities, we have investigated fcc and hcp elastic constants and high-symmetry fcc phonons in Fe and their pressure dependence. These results provide important information about the mechanical behavior of iron at high pressure, as well as providing valuable data for developing interatomic potentials. Recently, Stixrude and Cohen[10] used tight-binding calculations of fcc and hcp elastic constants at a single compressed volume in iron to argue that the inner core is elastically anisotropic and further showed that observed seismic travel-time anomalies are consistent with a model of the inner core composed of a nearly perfectly aligned aggregate of hcp crystals. Qualitatively, our calculations support their conclusions about elastic anisotropy in high-pressure fcc and hcp iron, although quantitatively, there are some differences in the calculated elastic constants.

The paper is organized as follows. Section II elaborates the computational approach used in our *ab initio* electronic-structure calculations. This section is followed by a presentation of our results for crystal-structure phase stabilities in Sec. III and our results for the elastic and vibrational properties of iron at high compression in Sec. IV. In Sec. V we discuss the development of many-body interatomic potentials for iron and our initial applications with them to full fcc and hcp phonon spectra. Finally, we present our conclusions in Sec. VI.

II. ELECTRONIC-STRUCTURE CALCULATIONS

The results presented below in Secs. III and IV on the structural, vibrational, and elastic properties of Fe all derive from accurate calculations of the electronic total energy for assumed static configurations of the ions. For each configuration considered, the total energy has been obtained from a fully self-consistent *ab initio* electronic-structure calculation. Both nonmagnetic (non-spin-polarized) and magnetic (spin-polarized with ferromagnetic ordering) treatments have been considered. Nonmagnetic calculations have been used for the elastic constants of fcc and hcp iron and also for the fcc Brillouin-zone-boundary phonons, since our primary interest here is the high-pressure region where ferromagnetism is suppressed in the close-packed phases. Magnetic calculations have been done for the bcc, fcc, bct, hcp, and dhcp crystal structures of iron, however, because ferromagnetism plays an important role in the overall phase diagram. All calculations have been performed with a full-potential, linear-muffin-tin-orbital (FP-LMTO) method,[11] which has previously been used to calculate elastic constants for both cubic[12] and hexagonal[13] d-transition metals. The present nonmagnetic calculations have been done in a similar manner, and are based on density-functional theory with the local-density approximation (LDA) to the exchange-correlation functional suggested by von Barth and Hedin.[14] All relativistic effects have been taken into account except the spin-orbit interaction for the valence electrons, where the scalar relativistic equations have been solved. The full Dirac equation has been solved for the core electrons. For the magnetic calculations, we have applied gradient corrections to the LDA, according to the generalized gradient approximation (GGA) developed by Perdew and co-workers,[15] since this improvement is essential to obtain the correct ground state at low pressure.

The FP-LMTO method employs a minimal basis set of muffin-tin orbitals[16] to treat both the large pseudocore or semicore states and the valence states. The calculations were done with one, fully hybridizing, energy panel in which basis orbitals corresponding to the semicore 3s and 3p states and to the valence 4s, 4p, 3d, and 4f states were defined. Two kinetic energy parameters (κ^2) appropriate for the tails of the 3s, 3p, and the valence states were used, i.e., six κ values in all. We found that this choice of a so-called double basis set was generally important. We also found that neglecting the semicore states in the basis set resulted, for instance, in an almost 10% lower X-point phonon (X phonon) frequency at about 35% compression for fcc Fe. Furthermore neglecting the 4f states in the valence energy bands increased the X-phonon frequency by a similar amount.

Structural energies have been obtained on the basis of GGA total-energy differences amongst the five solid phases considered. The total energy of each phase has been calculated at 12 volume points between ambient density and about twofold compression. In the case of the bct, hcp, and dhcp structures, the variation of total energy with c/a axial ratio has also been studied in certain regimes, as will be discussed in Sec. III. For the hcp structure ($c/a = 1.585$), the pressure P and bulk modulus B have also been calculated from volume derivatives of an analytic fit to the total-energy versus volume curve. This has likewise been done for the nonmagnetic LDA treatments of the fcc and hcp structures, where the total energy has been calculated at a smaller number of volumes. Figure 2 displays our GGA and LDA pressure-volume relations for hcp Fe together with room-temperature diamond-anvil-cell data[17] for the hcp ϵ phase, which has been measured to about 3 Mbar. The latter shows good agreement with our calculated GGA result, while our LDA result systematically underestimates the pressure by about

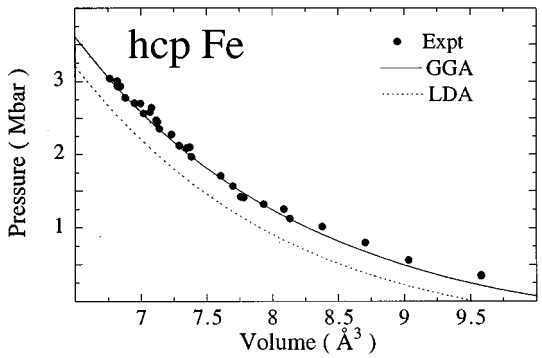

FIG. 2. Calculated GGA and LDA pressure-volume relations for hcp Fe compared with room-temperature static compression data of Ref. 17.

25–40 GPa. As a consequence of the latter, the LDA bulk modulus at a given volume is also underestimated. This shortcoming is not extended to the elastic constants in general, however. In fact, test calculations on the fcc shear constants, C' and C_{44}, demonstrate that the LDA and GGA treatments give very similar results for these quantities.

Elastic constants and phonon frequencies have been obtained from changes in the LDA total energy with applied strain or lattice distortion. For fcc Fe, the C' and C_{44} shear elastic constants together with the longitudinal and transverse phonons at the X and L symmetry points have been calculated at three volumes: 9.70, 7.55, and 6.17 Å^3. The largest of these volumes represents an 18% compression from ambient density, but is near the nonmagnetic equilibrium point as calculated in the LDA. For the hcp phase of iron, we have evaluated the five elastic constants C_{11}, C_{12}, C_{13}, C_{33}, and C_{44} at these same volumes. Rigorous methods to calculate the cubic[12] and hexagonal[13] elastic constants have been well described in previous studies and we do not repeat those discussions here. The calculation of phonon frequencies is relatively recent in the context of the FP-LMTO method, however, so in this case we describe our actual procedure, with additional details given in Appendix A. The phonon calculations employ the so-called frozen-phonon method,[18] in which the total energy is calculated for static atomic displacements consistent with the phonon mode under consideration. This technique has been applied here to four zone-boundary phonons, the longitudinal and transverse L and X phonons. For these modes, it suffices to study a doubled unit cell for the fcc structure. One of the two atom types in this cell is kept fixed while the other is displaced according to a longitudinal or transverse phonon. For sufficiently small displacements, the total energy increase due to such a distortion, ΔE, is related to the zone-boundary phonon frequency $\omega_{\mathbf{q}}$ by the harmonic relation

$$\Delta E = \tfrac{1}{2} M (u_{\mathbf{q}} \omega_{\mathbf{q}})^2, \tag{1}$$

where M is the atomic mass for Fe and $u_{\mathbf{q}}$ is the amplitude of the displacement. Here $\omega_{\mathbf{q}}$ is the angular phonon frequency corresponding to normalized wave vectors $\mathbf{q}=(1,0,0)$ (X phonons) or $\mathbf{q}=(\frac{1}{2},\frac{1}{2},\frac{1}{2})$ (L phonons). The X phonons arise from vibrations of the (100) planes in the fcc crystal, whereas the L phonons arise from vibrations of the (111) planes. In addition to the equilibrium configuration, the total energy for three displacements were calculated for each phonon frequency and volume, so that the harmonic part of ΔE could be accurately extracted. The phonon amplitudes $u_{\mathbf{q}}$ were chosen so that ΔE was within an interval of about $0.05-5.0$ mRy/atom at all volumes. Since the phonon frequencies increase as the metal is compressed, the displacement amplitude was decreased for the smaller volumes and the values for $u_{\mathbf{q}}$ ranged from 0.1 to 2 % of the fcc lattice parameter depending on the actual compression.

One of the most problematic issues in such *ab initio* total-energy calculations is the convergence of each result with respect to the k-point sampling used in performing required sums over the Brillouin zone (BZ). In this work, the energy eigenvalues were calculated for various numbers of k points in the BZ and the sampling was done with the special k-point method.[19] When comparing the total energies for the bcc, fcc, bct, hcp, and dhcp crystal structures, relatively few k points were needed to converge the results. For the bcc, fcc, and bct structures we used a total of 150 k points in the irreducible wedge of the BZ (IBZ; 1/16 of the full body-centered-tetragonal BZ), whereas for the hcp and dhcp structures the total energies were sufficiently converged for 162 k points in their IBZ (1/12 of the full simple-hexagonal BZ). For the calculation of the elastic constants and zone-boundary phonons we used substantially more k points. In our previous work on elastic constants,[12] we found that a larger number of k points is needed to accurately obtain the small differences in the total energy associated with the small distortions involved. These earlier calculations[12] were done at ambient conditions whereas the present study concerns iron under high compression and that makes it considerably harder to converge the total energy with respect to the number of k points. This is true because as the real-space volume is decreased upon compression, the reciprocal-space BZ volume is increased and hence more k points are needed to maintain the same k-point density in Fourier space. For the fcc tetragonal shear constant C', we have used up to 2119 k points in the IBZ, whereas for the C_{44} elastic constant the largest number of k points (for the most compressed volume) was 2176 in the IBZ. Apart from the larger number of k points used in the present calculations for C' and C_{44}, they are similar to our previous studies of elastic constants for cubic d-transition metals. The hcp elastic constants were calculated for somewhat less number of k points, but never less than about 2000 k points in the full BZ were used.

For the same reason as for the calculations of the elastic constants, the k-point convergence of the phonon frequencies was carefully examined for fcc Fe. This convergence was never worse than about 4%, but mostly less than 2%. For the longitudinal and transverse X phonons, the number of k points used in the IBZ was 936 and 1872, respectively. For the L phonons a somewhat smaller k-point set was needed and the number of k points used in the IBZ was 1088 for the longitudinal and 2048 for the transverse L phonons, respectively.

III. CRYSTAL STRUCTURE PHASE STABILITIES

At low pressure, the crystallographic phase stabilities of fcc, bcc, and hcp Fe have been studied theoretically by many

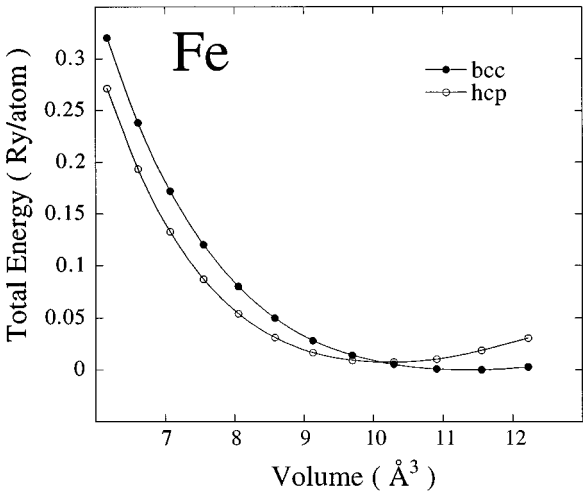

FIG. 3. Calculated total energies for the bcc and hcp crystal structures of Fe as a function of volume.

previous workers, especially with regard to the role of magnetism in explaining the observed phase diagram.[20,21] In particular, it is well known that the bcc α phase is stabilized by ferromagnetism at ambient conditions. It is also well known, however, that magnetic electronic-structure calculations based on the local-density approximation to exchange and correlation predict the wrong ground state for Fe (fcc instead of bcc). Fortunately, this problem has recently been solved[22] by the introduction of gradient corrections to the LDA and our calculations of the crystal-structure phase stabilities presented below, therefore, incorporate a state-of-the-art GGA version of this improvement.[15,23]

Figure 3 displays our calculated GGA total energies for the bcc and hcp Fe structures as a function of volume. In Fig. 4 we also show the energy differences between the fcc, bct, hcp, and, dhcp crystal structures and bcc, such that the bcc result defines the zero of energy on this plot. The bct, hcp, and dhcp results in this plot are for assumed c/a axial

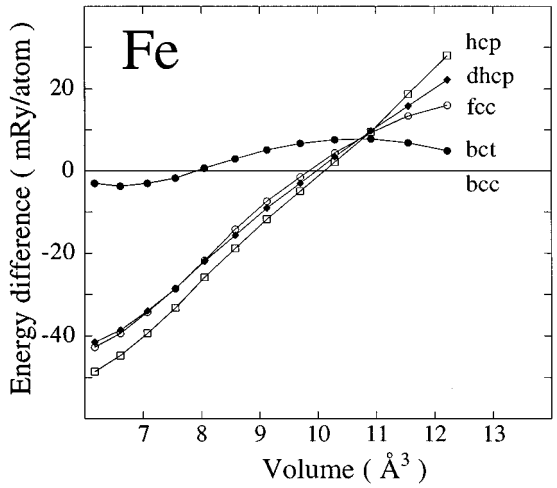

FIG. 4. Calculated total energies for the fcc, bct, hcp, and dhcp structures of Fe relative to the bcc result, which defines the zero of energy.

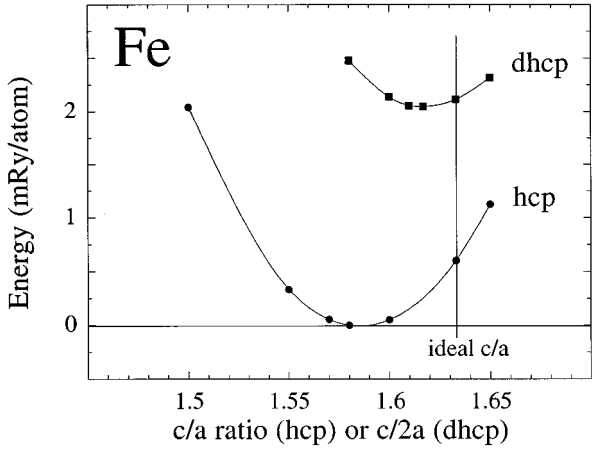

FIG. 5. Relative total energies for the hcp and dhcp crystal structures of Fe calculated as a function of c/a (hcp) and $c/2a$ (dhcp), at about 9.8 Å^3 (a volume representative for the ϵ' phase).

ratios of 0.875, 1.585, and 3.234, respectively, which minimize the total energy for some or all of the volume range considered, as discussed below. Notice that the hcp energy crosses below the bcc energy just above 10 Å^3. The corresponding bcc→hcp transition pressure is calculated to be about 10 GPa, in close agreement with both experiment and other theoretical results.[9,22] Clearly, at zero temperature these are the only two structures which are stabilized, and at high pressure hcp is predicted to be the ground state to beyond 4 Mbar.

At high temperatures and pressures, such as in the earth's core, there might be others of these phases which are stabilized by magnetic or phonon entropy effects, as suggested by the recent experimental findings summarized in Fig. 1 and discussed above. In particular, the discovery of a high-temperature dhcp (Refs. 5 and 6) phase has encouraged us to study the relationship between the dhcp and hcp structures in more detail. In Fig. 5 we show the total energy for the dhcp and hcp structures as a function of their c/a ratios at a volume of about 9.8 Å^3, which is representative of the observed dhcp phase. The dhcp calculations were done for both ferromagnetic and anti-ferromagnetic ordering and in each case the ferromagnetic calculation gave a lower total energy, so these are the results plotted in Fig. 5. Only the dhcp structure maintains a finite magnetic moment at this volume, however, as the hcp ferromagnetic energies converge to the nonmagnetic values. The hcp results show a single minimum in the total energy for a $c/a = 1.585$, close to the value observed for the ϵ phase of iron ($c/a = 1.60$). The calculated dhcp total energy is minimized for a $c/2a = 1.617$ and lies only about 2 mRy/atom (corresponding to 315 K) above the hcp energy minimum. The calculated value of 3.234 for the c/a ratio in dhcp Fe is also remarkably close to the value of 3.233 measured by Yoo *et al.*[6] at the same volume. In both structures the c/a ratio is significantly lower than the ideal value, which is 1.633 for hcp and 3.266 for dhcp.

The appearance of hcp and dhcp phases in Fe with non-ideal values for the c/a ratio at high pressure is interesting and has motivated us to also study the relationship between the bcc and bct phases in some detail. The bct crystal struc-

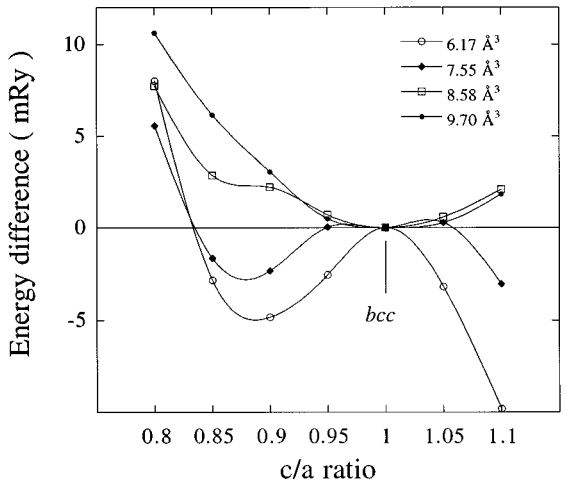

FIG. 6. Calculated total energy for the bct crystal structure of Fe along the Bain transformation path at four different volumes. For $c/a=1$ the bct structure is identical to the bcc structure. The energies are shifted so that the bcc energy is zero for each volume.

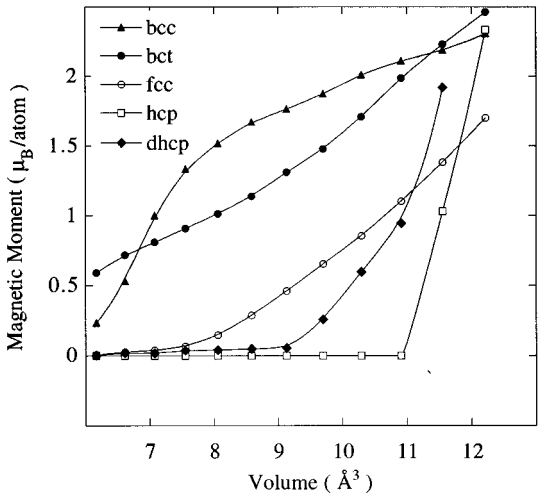

FIG. 7. Magnetic moment calculated as a function of volume for five crystal structures of Fe.

ture can be viewed as a tetragonal distortion, i.e., a shift in the c/a ratio, of either the bcc ($c/a=1$) or the fcc ($c/a=\sqrt{2}$) structure. The transformation path defined by the c/a parameter joining those structures is called the Bain transformation path.[24] In Fig. 6 we show this Bain path for Fe in the vicinity of $c/a=1$ at four separate volumes. At large volumes (>9Å^3), the bct energy is minimum for the bcc structure and there is only one metastable phase, namely the fcc structure ($c/a=\sqrt{2}$, not shown in Fig. 6). However, as the compression increases and the magnetic moment in iron is suppressed, the bcc structure becomes unstable with respect to a tetragonal distortion and a bct minimum with a $c/a\simeq 0.875$ develops. This occurs above about 2 Mbar in pressure. However, as can be seen in Fig. 4, even though the bct energy becomes lower than the bcc energy at high compression, it remains considerably higher than the fcc, hcp, and dhcp energies.

Additional insight about high-pressure and high-temperature phase stability of Fe is revealed by examining the calculated magnetic moments. Figure 7 shows the magnetic moment for the five structures considered here as a function of volume. It is clear that in the closed-packed structures (fcc, hcp, and dhcp) the magnetism is already suppressed at moderate pressures, whereas for the bcc and bct structures the magnetic moment remains significant even at high compression. Physically, this can be understood from the pronounced double-peak feature in the electronic d-density of states for these latter phases, which provides a particularly favorable situation for retaining a magnetic moment. Comparing the magnetic moment in the dhcp and hcp structures reveals that at volumes relevant to the observed ϵ' phase of Fe (Ref. 6) (about 9.3 to 10.1 Å^3), the dhcp structure still has a substantial net magnetic moment ($\sim 0.3\mu_B$/atom at 9.8 Å^3), while in the hcp structure it has completely vanished. This suggests that the ϵ' phase may be stabilized at high temperature by magnetic entropy and a possible temperature-induced enhancement of the magnetic moment in the manner discussed previously for the fcc γ phase.[21] Such a scenario is consistent with the intermediate position of dhcp between hcp and fcc both in calculated energy and magnetic moment as well as in temperature location on the observed phase diagram. This scenario is also consistent with the observation of Yoo *et al.*[6,7] that the dhcp ϵ' phase vanishes at high pressure above 50 GPa, since the calculated magnetic moment is reduced to near zero in that regime. Finally, it is interesting to note that the metastable bct phase displays the largest magnetic moment at very high compression, corresponding to pressures above 2 Mbar. Thus while we can probably rule out the bcc phase from the high-pressure phase diagram of iron, the bct phase cannot be so excluded and possibly the α' phase in Fig. 1 is bct instead of bcc.

IV. ELASTIC CONSTANTS AND PHONONS

In this section we next turn to the elastic and vibrational properties of nonmagnetic fcc and hcp iron relevant to the earth's core. Comparatively little fundamental theoretical work has been done on these properties outside of the recent elastic constant calculations of Stixrude and Cohen.[10] These authors performed an elaborate tight-binding fit to *ab initio* GGA electronic structure and total-energy calculations on compressed iron and then used the tight-binding parameters in turn to calculate fcc and hcp elastic constants at a single compressed volume near earth-core conditions. We, on the other hand, have calculated *ab initio* LDA elastic constants and phonons directly at a series of three volumes spanning both low and high pressures in fcc and hcp Fe.

TABLE I. Calculated elastic constants and phonons for nonmagnetic fcc Fe under compression. Volumes are in Å^3; pressures, bulk moduli, and elastic constants are in Mbar; and phonon angular frequencies (ω) are in 10^{12} rad/s.

Volume	P	B	C'	C_{44}	L[100]	T[100]	L[111]	T[111]
9.70	-0.02	3.30	1.18	2.86	39.8	40.0	56.1	30.7
7.55	1.43	8.92	2.06	5.80	84.2	63.3	100	45.2
6.17	4.06	17.6	3.36	9.50	123	85.6	138	60.1

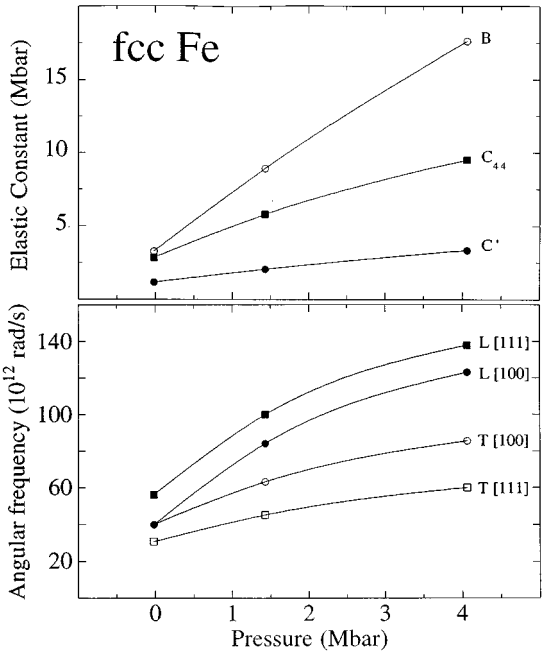

FIG. 8. The calculated pressure dependence of the elastic constants (upper panel) and zone-boundary phonons (lower panel) for nonmagnetic fcc Fe. $L[100]$ and $T[100]$ denotes the longitudinal and transverse X phonons; $L[111]$ and $T[111]$ denotes the longitudinal and transverse L phonons.

Our calculated fcc results are summarized in Table I and Fig. 8, while our hcp results are elaborated in Table II and Fig. 9. In the tables, we list the calculated pressure P and bulk modulus B in addition to the elastic-constant and phonon data. For the hcp calculations, we have actually used the ideal c/a axial ratio of 1.633 here instead of the theoretical value of 1.585, but we do not believe that the difference is significant. The calculated zone-boundary phonons in Table I are the longitudinal and transverse X phonons, $L[100]$ and $T[100]$, and L phonons, $L[111]$ and $T[111]$. Formally, our elastic constants are the stress-strain coefficients defined by Wallace,[25] so that for the cubic-symmetry, fcc case, the familiar equilibrium relations

$$C' = \tfrac{1}{2}(C_{11} - C_{12}) \tag{2}$$

and

$$B = \tfrac{1}{3}(C_{11} + 2C_{12}) \tag{3}$$

continue to hold at all pressures and C' and B alone determine C_{11} and C_{12}. Qualitatively, there is reasonable overall consistency between our calculated fcc and hcp elastic constants and those of Stixrude and Cohen.[10] When we interpolate our values to their volume (7.13 Å^3), we find quantitative agreement to about 5–15%, with two exceptions. The exceptions are C' for the fcc structure and C_{12} for the hcp structure for which our values are about 33% lower than theirs. The reasons for the latter discrepancies are not understood at present, but are possibly significant with respect to quantitative modeling of the inner core.

Our calculated elastic constants are everywhere positive and smoothly increasing functions of compression. This implies full mechanical stability of the fcc and hcp structures over the entire pressure range considered. For fcc Fe, B, C', and C_{44} all increase proportionally with the applied pressure, with B increasing faster than C_{44} and C', as shown in the upper panel of Fig. 8. Likewise, C_{44} increases more rapidly than C' upon compression implying that fcc Fe is increasingly anisotropic, with regard to the propagation of elastic waves, as a function of pressure. The fact that the earth's core shows a large degree of elastic anisotropy has indeed been suggested by both theory and experiment.[10,26]

TABLE II. Calculated elastic constants for nonmagnetic hcp Fe under compression. Volumes are in Å^3 and pressures, bulk moduli, and elastic constants are in Mbar.

Volume	P	B	C_{11}	C_{12}	C_{13}	C_{33}	C_{44}
9.70	-0.01	3.48	6.38	1.90	2.18	6.06	1.78
7.55	1.40	8.98	15.1	4.60	6.73	14.5	4.14
6.17	4.02	17.7	27.5	8.93	14.7	27.8	7.67

It is also worthwhile to note that the tetragonal shear constant C' is defined by a small distortion of the c/a parameter along the Bain path and consequently is proportional to the local curvature on the path at $c/a = \sqrt{2}$ for the fcc structure and at $c/a = 1$ for the bcc structure. Clearly, fcc Fe becomes more stable with respect to such a distortion as the pressure increases since C' increases with pressure. This is in direct contrast to the behavior of bcc Fe which becomes unstable for a tetragonal distortion and hence displays negative Bain-path curvature and a negative C' at sufficiently high pressure, as can be seen from Fig. 6.

The lower panel of Fig. 8 shows the pressure dependence of the zone-boundary phonons for nonmagnetic fcc Fe. The longitudinal modes are seen to increase faster with increasing pressure than the transverse modes, with an interesting crossing of $L[100]$ and $T[100]$ at low pressure. Unfortunately, there are no available experimental measurements or comparable theoretical results with which to make comparison here. To our knowledge similar calculations for high-pressure Fe have not been done before.

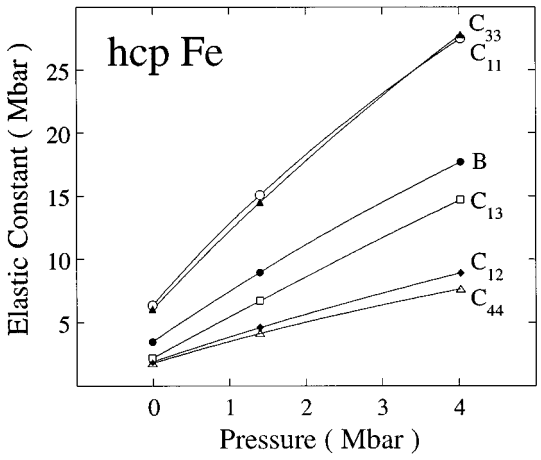

FIG. 9. The calculated pressure dependence of the elastic constants for nonmagnetic hcp Fe.

V. INTERATOMIC POTENTIALS AND FULL PHONON SPECTRA

In this section we turn our attention to the development of corresponding many-body interatomic potentials for iron, with which melting and other high-temperature properties can be calculated. Our starting point here is first-principles generalized pseudopotential theory (GPT) which provides a rigorous real-space expansion of the total energy of a bulk transition metal in the form[27]

$$E_{\rm tot}(\mathbf{R}_1 \ldots \mathbf{R}_N) = NE_{\rm vol}(\Omega) + \frac{1}{2}{\sum_{i,j}}' v_2(ij) + \frac{1}{6}{\sum_{i,j,k}}' v_3(ijk) + \frac{1}{24}{\sum_{i,j,k,l}}' v_4(ijkl), \tag{4}$$

where $\mathbf{R}_1 \ldots \mathbf{R}_N$ denote the positions on the N ions in the metal, Ω is the atomic volume, and the prime on each sum over ion positions excludes all self-interaction terms where two indices are equal. The leading volume term in this expansion, $E_{\rm vol}$, as well as the interatomic potentials v_2, v_3, and v_4 are volume dependent, but *structure independent* and thus *transferable* to all bulk ion configurations, ordered or disordered. At constant volume Ω, the radial-force pair potential v_2 is a one-dimensional function of the ion-ion separation distance $R_{ij}=|\mathbf{R}_i-\mathbf{R}_j|$:

$$v_2(ij) = v_2(R_{ij};\Omega), \tag{5}$$

while the angular-force triplet potential v_3 and quadruplet potential v_4 are, respectively, the three- and six-dimensional functions

$$v_3(ijk) = v_3(R_{ij},R_{jk},R_{ki};\Omega) \tag{6}$$

and

$$v_4(ijkl) = v_4(R_{ij},R_{jk},R_{kl},R_{li},R_{ki},R_{lj};\Omega). \tag{7}$$

The GPT total-energy expansion (4) has been developed within the nonmagnetic LDA framework of density-functional theory and our applications to iron are all confined to this limit. Explicit *ab initio* expressions for $E_{\rm vol}$, v_2, v_3, and v_4 have been obtained in terms of weak pseudopotential and d-state matrix elements and are given in Ref. 27. In the full GPT, however, these functionals are nonanalytic quantities, so that the multidimensional potentials v_3 and v_4 cannot be readily tabulated and used for applications purposes. This problem has been overcome by the development of a companion model GPT or MGPT (Ref. 28) in which canonical d bands and other simplifications are introduced in order to achieve analytic forms for the potentials v_3 and v_4, as well as analytic d-state components of v_2. In the MGPT both the formal character of Eqs. (4)–(7) and the dominant physics of the full theory are retained, while the more approximate nature of the potentials is compensated for by allowing variable coefficients to the d-state components of v_2, v_3, and v_4, which in turn can be adjusted to *ab initio* data. It is through this latter mechanism that we here use the above LDA FP-LMTO elastic constant and phonon data in developing MGPT potentials for iron.

In the following we consider a specific, representative scheme for obtaining iron MGPT potentials. We have been guided here by both past experience on bcc transition metals[28] and by our desire to produce potentials which will be optimally effective for the melting calculation at high pressure. We have also taken advantage of the availability of additional LDA LMTO calculational data on nonmagnetic iron[8] obtained in the atomic-sphere approximation (ASA). The MGPT formalism provides a maximum of five d-state potential coefficients which can be adjusted as a function of volume. A sixth parameter can be made available by allowing the volume term $E_{\rm vol}$ also to be variable. This additional freedom is used to enforce the rigorous compressibility sum rule, which ensures that the bulk modulus is the same whether calculated from volume derivatives of $E_{\rm tot}$ or from position derivatives of the potentials v_2, v_3, and v_4 at constant volume. We have determined the remaining five parameters by fitting them, as a function of volume, to a selected blend of LMTO-ASA and FP-LMTO data for nonmagnetic fcc iron. Two of these parameters have been constrained by LMTO-ASA results for the bulk modulus and the bcc-fcc energy difference.[8] In this regard, the LMTO-ASA values of the bulk modulus are preferred over the FP-LMTO values because the ASA effectively compensates for the systematic LDA underestimates of pressure and bulk modulus noted above in connection with Fig. 2. As a consequence, the resulting MGPT room-temperature isotherm obtained via Eq. (4) for hcp iron is in good accord with experiment. At the same time, the constraint of the bcc-fcc energy difference ensures a qualitatively correct description of structural energies for the hcp, fcc, bct, and bcc phases in the nonmagnetic limit. In particular, hcp is properly the ground state for all volumes and bcc is unstable with respect to a tetragonal distortion, yielding a lower-energy metastable bct phase for $c/a \simeq 0.85$. It should be noted, however, that the positive fcc-hcp energy difference is quantitatively underestimated in the MGPT due to its neglect of higher-order multi-ion d-state contributions beyond four-body interactions. The final three MGPT parameters have been constrained by the present FP-LMTO elastic-constant and phonon data. This has been done by exactly fitting the average fcc phonon frequency $(L[100]+2T[100]+L[111]+2T[111])/6$ as a function of volume, while simultaneously maximizing the agreement for the four individual phonon frequencies and two elastic constants (C_{44} and C'). The idea here is that the average phonon frequency should be approximately proportional to the Debye temperature, which in turn controls the melting temperature. Figure 10 compares the resulting MGPT phonons and elastic constants with the *ab initio* FP-LMTO data. The MGPT readily accommodates all quantities except the $L[111]$ phonon frequency, which is systematically underestimated. As desired, however, the level of agreement improves with increasing compression and the maximum error is only 12% at the smallest volume considered.

The MGPT potentials so determined have been used to calculate complete quasiharmonic phonon spectra, Debye temperatures, and free energies for the nonmagnetic fcc, hcp, and bct Fe phases as a function of compression. The fcc and hcp structures are found to be everywhere mechanically stable, with real phonon frequencies over the whole volume

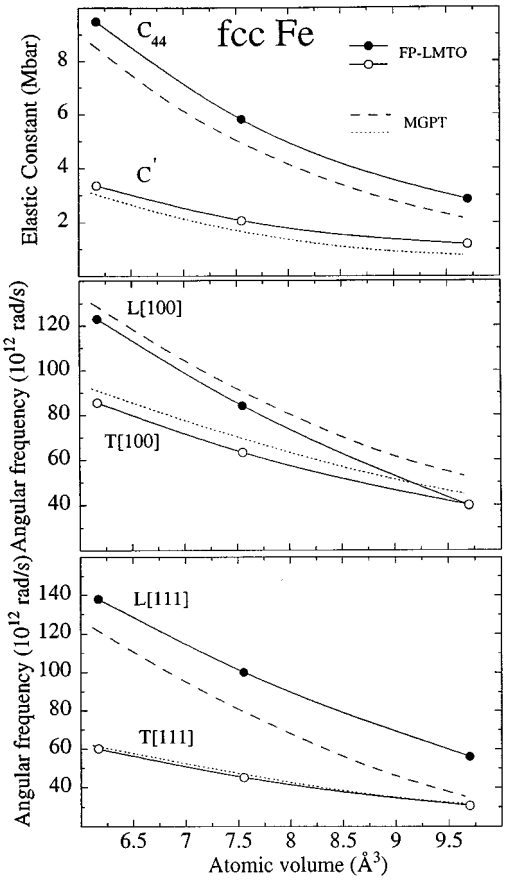

FIG. 10. Comparison of elastic constants and phonons for nonmagnetic fcc Fe calculated with the FP-LMTO and MGPT methods. Upper panel: C_{44} and C' elastic constants; central panel: X-point phonons; lower panel: L-point phonons.

range considered (6.11 to 9.65 Å^3), while the bct structure becomes mechanically unstable for volumes greater than about 8.23 Å^3. The latter outcome, however, is very sensitive to the details of the potentials, and the mechanical stability of the true *magnetic* bct structure of iron remains to be investigated. Representative fcc and hcp phonon spectra at high compression are displayed in Figs. 11 and 12, respectively. For each phonon spectra considered, a Debye temperature Θ_D is defined in terms of the zero-point vibrational energy,

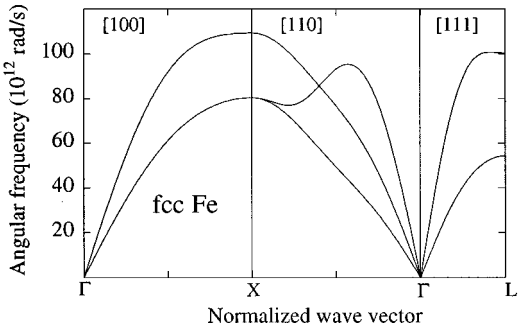

FIG. 11. Calculated MGPT phonon spectrum of nonmagnetic fcc Fe at a volume of 6.82 Å^3, corresponding to a zero-temperature pressure of 2.8 Mbar.

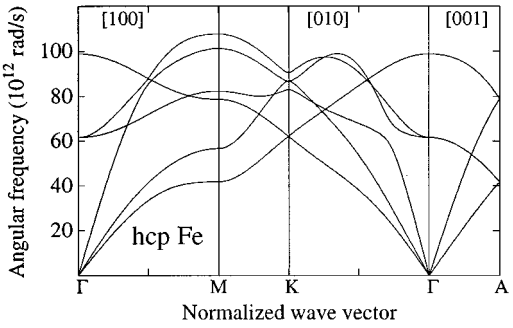

FIG. 12. Calculated MGPT phonon spectrum of nonmagnetic hcp Fe at a volume of 6.82 Å^3, corresponding to a zero-temperature pressure of 2.8 Mbar.

$$E_{\rm ph}^0 = \frac{1}{2N}\sum_{\mathbf{q}} \hbar\omega_{\mathbf{q}}, \tag{8}$$

by the Debye relation $E_{\rm ph}^0 = 9/8 k_B \Theta_D$, where the sum in Eq. (8) is over all phonon modes in the first Brillouin zone of the lattice. The calculated volume dependence of Θ_D is illustrated in Fig. 13 for fcc, hcp, and bct Fe. Note that the Debye temperatures of the fcc and hcp structures are almost the same at all volumes, while that of the bct structure is considerably higher. Corresponding phonon free energies have been calculated to 17 500 K in temperature at each volume considered for all three phases. The hcp structure maintains the lowest free energy at all volumes and temperatures, so at least in the nonmagnetic, quasiharmonic limit, we conclude that iron will melt out of this structure.

VI. CONCLUSIONS

Five representative crystal structures for iron have been studied as a function of compression by means of *ab initio* FP-LMTO density-functional calculations, and the results have some clear implications for the high-pressure, high-temperature phase diagram of this metal. We find that the recently observed dhcp structure is likely to be energetically accessible at high temperature for pressures below about 50 GPa due to its ferromagnetic character. This conclusion is consistent with dhcp as the proposed $\epsilon'-$Fe phase of Yoo *et al.*,[6,7] but not with dhcp being the proposed $\beta-$Fe phase[2,5] above 50 GPa. We further find that as the magnetism in bcc

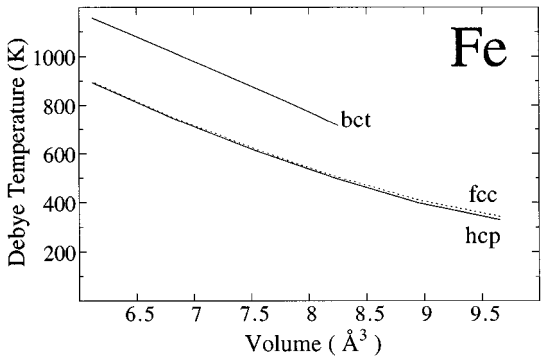

FIG. 13. Calculated MGPT Debye temperatures for nonmagnetic fcc, hcp, and bct Fe as a function of volume.

TABLE III. Atomic positions in the doubled fcc cell for the longitudinal and transverse X phonons ($L[100]$ and $T[100]$) and L phonons ($L[111]$ and $T[111]$) represented in their Bravais lattice basis (see text). The quantity **q** is the normalized phonon wave vector.

	$L[100]$	$T[100]$	$L[111]$	$T[111]$
Atom 1	(0,0,0)	(0,0,0)	(0,0,0)	(0,0,0)
Atom 2	$(\frac{1}{2},\frac{1}{2},\frac{1}{2}-2u)$	$(\frac{1}{2}-2u,\frac{1}{2}-2u,\frac{1}{2})$	$(-2u,-2u,\frac{1}{2}+u)$	$(2u,0,\frac{1}{2})$
q	(1,0,0)	(0,0,1)	(1,1,−1)	(0,1,1)

Fe is suppressed at high pressure above 2 Mbar, this phase becomes mechanically unstable and a metastable bct phase is developed in its place. Consequently, bcc is an unlikely candidate for the proposed α' phase of iron at earth-core conditions, and our calculations support other researchers' conclusions in this regard.[8,9] The bct phase, on the other hand, is interesting and deserves more attention. Although this phase is considerably higher in energy than the hcp ground state, it retains a substantial magnetic moment even at megabar pressures. A scenario where the bct is stabilized at high pressure and high temperature by magnetic entropy effects cannot be entirely ruled out at present, and it remains possible that this is the α' phase. It is, therefore, our intention to investigate the elastic and vibrational properties of magnetic bct Fe in the future.

For the nonmagnetic fcc and hcp phases of Fe, we have also done a series of *ab initio* FP-LMTO calculations in order to determine their elastic constants, and for the fcc phase the zone-boundary phonons as well, as a function of compression. The elastic constants should be useful in the future for detailed modeling of the inner core of the earth. The fcc data has been used in the present paper to develop multi-ion MGPT interatomic potentials, which in turn have been applied to obtain complete fcc and hcp phonon spectra and Debye temperatures. These same potentials are currently being used in molecular dynamics simulations aimed at determining the high-pressure melting curve of iron, and these studies will be reported at a later date.

ACKNOWLEDGMENTS

We would like to thank O. Eriksson, J. Trygg, L. Fast, and C.-S. Yoo for valuable discussions. This work was performed under the auspices of the U.S. Department of Energy by the Lawrence Livermore National Laboratory under Contract No. W-7405-ENG-48.

APPENDIX

In this appendix, we review some technical details regarding the calculation of the zone-boundary phonons utilizing the frozen-phonon method for a metal in the fcc crystal structure. The phonons of interest are the X and L phonons that arise from vibrations of the (100) and (111) planes of the fcc cell, respectively. For these phonons it suffices to study a doubled unit cell, spanned by the Bravais lattice vectors for the X phonons,

$$\mathbf{R}=\begin{pmatrix} 0 & \frac{1}{2} & \frac{1}{2} \\ 0 & -\frac{1}{2} & \frac{1}{2} \\ 1 & 0 & 0 \end{pmatrix}, \tag{A1}$$

and for the L phonons

$$\mathbf{R}=\begin{pmatrix} 0 & \frac{1}{2} & \frac{1}{2} \\ \frac{1}{2} & 0 & \frac{1}{2} \\ 1 & 1 & 0 \end{pmatrix}, \tag{A2}$$

in units of the lattice constant a. The doubled cell has two atoms with equilibrium positions (0,0,0) and $(\frac{1}{2},\frac{1}{2},\frac{1}{2})$ for the X phonons whereas for the L phonons the positions are (0,0,0) and $(0,0,\frac{1}{2})$. These atomic positions are here represented in their respective Bravais lattice coordinates. In the frozen-phonon method the energy increase (ΔE) associated with a phonon displacement, $u_{\mathbf{q}}=u|\mathbf{q}|a$, defined by the normalized vector **q**, is calculated and the corresponding angular frequency can be obtained by means of Eq. (1). In practice we let one of the atoms be fixed and displace the other by an amount $2u$ in the specific direction given by **q** (in the Cartesian coordinates). Table III shows the **q**'s corresponding to the four phonon modes and also the (nonequilibrium) atomic positions governed by those modes. By calculating total energies and extracting ΔE, the angular frequency can be obtained from the harmonic relation

$$\omega_{\mathbf{q}}=\sqrt{\frac{2\Delta E}{Mu^2|\mathbf{q}|^2a^2}}. \tag{A3}$$

[1] See, for example, *High-Pressure Science and Technology-1993*, edited by S.C. Schmidt, J.W. Shaner, G.A. Samara, and M. Ross (American Institute of Physics, New York, 1994), pp. 887–966.

[2] R. Boehler, Nature (London) **363**, 534 (1993); S.K. Saxena, G. Shen, and P. Lazor, Science **260**, 1312 (1993).

[3] J.M. Brown and R.G. McQueen, Geophys. Res. Lett. **7**, 533 (1980); J. Geophys. Res. **91**, 7485 (1986).

[4] M. Ross, D.A. Young, and R. Grover, J. Geophys. Res. **95**, 21713 (1990).

[5] S.K. Saxena, L.S. Dubrovinsky, P. Häggkvist, Y. Cerenius, G. Shen, and H.K. Mao, Science **269**, 1703 (1995).

[6] C.S. Yoo, P. Söderlind, J.A. Moriarty, and A. Campbell, Phys. Lett. A (to be published).

[7] C.S. Yoo, J. Akella, A.J. Campbell, H.K. Mao, and R.J. Hemley, Science **270**, 1473 (1995).
[8] J.A. Moriarty, in *High-Pressure Science and Technology-1993* (Ref. 1), p. 233.
[9] L. Stixrude, R.E. Cohen, and D.J. Singh, Phys. Rev. B **50**, 6442 (1994).
[10] L. Stixrude and R.E. Cohen, Science **267**, 1972 (1995).
[11] J.M. Wills (unpublished); J.M. Wills and B.R. Cooper, Phys. Rev. B. **36**, 3809 (1987); D.L. Price and B.R. Cooper, *ibid.* **39**, 4945 (1989).
[12] J.M. Wills, O. Eriksson, P. Söderlind, and A.M. Boring, Phys. Rev. Lett. **68**, 2802 (1992); P. Söderlind, O. Eriksson, J.M. Wills, and A.M. Boring, Phys. Rev. B **48**, 5844 (1993); P. Söderlind, R. Ahuja, O. Eriksson, B. Johansson, and J.M. Wills, *ibid.* **50**, 5918 (1994).
[13] L. Fast, J.M. Wills, B. Johansson, and O. Eriksson, Phys. Rev. B **51**, 17 431 (1995).
[14] U. von Barth and L. Hedin, J. Phys. C **5**, 1629 (1972); J.F. Janak, V.L. Moruzzi, and A.R. Williams, Phys. Rev. B **12**, 1257 (1975).
[15] J.P. Perdew, J.A. Chevary, S.H. Vosko, K.A. Jackson, M.R. Pederson, and D.J. Singh, Phys. Rev. B **46**, 6671 (1992).
[16] H.L. Skriver, *The LMTO Method* (Springer-Verlag, Berlin, 1984).
[17] H.K. Mao, Y. Wu, L.C. Chen, J.F. Shu, and A.P. Jephcoat, J. Geophys. Res. **95**, 21 737 (1990).
[18] K.-M. Ho, C.L. Fu, B.N. Harmon, W. Weber, and D.R. Hamann, Phys. Rev. Lett. **49**, 673 (1982).
[19] D.J. Chadi and M.L. Cohen, Phys. Rev. B **8**, 5747 (1973).
[20] For example, M.V. You, V. Heine, A.J. Holden, and P.J. Lin-Chung, Phys. Rev. Lett. **44**, 1282 (1980).
[21] H. Hasegawa and D.G. Pettifor, Phys. Rev. Lett. **50**, 130 (1983).
[22] P. Bagno, O. Jepsen, and O. Gunnarsson, Phys. Rev. B **40**, 1997 (1989); B. Barbiellini, E.G. Moroni, and T. Jarlborg, J. Phys. Condens. Matter **2**, 7597 (1990); T.C. Leung, C.T. Chan, and B.N. Harmon, Phys. Rev. B **44**, 2923 (1991); D.J. Singh, W.E. Pickett, and H. Krakauer, *ibid.* **43**, 11 628 (1991).
[23] P. Söderlind, O. Eriksson, J.M. Wills, and B. Johansson, Phys. Rev. B **52**, 4420 (1995).
[24] E.C. Bain, Trans. AIME **70**, 25 (1924).
[25] D.C. Wallace, *Thermodynamics of Crystals* (Wiley, New York, 1972). At finite pressure, our C_{ij} elastic constants correspond to Wallace's B_{ij} stress-strain coefficients.
[26] J. Tromp, Nature (London) **366**, 678 (1993); X. Song and D.V. Helmberger, J. Geophys. Res. Lett. **20**, 2591 (1993).
[27] J.A. Moriarty, Phys. Rev. B **38**, 3199 (1988).
[28] J.A. Moriarty, Phys. Rev. B **42**, 1609 (1990); **49**, 12 431 (1994).